ELSEVIER

Ceramics International 26 (2000) 565–569

CERAMICS INTERNATIONAL

Three-dimensional phase diagram of the $Pb(Zr,Ti)O_3$ system under hydrostatic pressure

S. Hoon Oh, Hyun M. Jang*

Department of Materials Science and Engineering, and Laboratory for Physics/Chemistry of Dielectric Materials, Pohang University of Science and Technology (POSTECH), Pohang 790-784, South Korea

Received 15 October 1998; received in revised form 26 October 1998; accepted 28 August 1999

Abstract

The rotostrictive coefficient of $F_{R(LT)}-F_{R(HT)}$ phase transition in the rhombohedral $Pb(Zr,Ti)O_3$ (PZT) has been evaluated. Using a phenomenological thermodynamic formalism a shift of the thermodynamically stable phase fields of PZT under hydrostatic pressure has been predicted. The para-ferroelectric transition temperature increases, the $F_{R(LT)}$–$F_{R(HT)}$ transition temperature decreases, and the composition of the morphotropic phase boundary (MPB) moves towards the tetragonal phase field with increasing tensile hydrostatic pressure. Contrary to these, opposite trends were predicted with increasing compressive pressure. Three-dimensional phase diagrams of PZT system using composition, pressure and temperature as the three independent thermodynamic variables have been computed.

Keywords: Phase diagram of $Pb(Zn,Ti)O_3$; Hydrostatic pressure

1. Introduction

The lead zirconate–titanate (PZT) solid solution system contains a number of important compositions used in the electronics industry [1]. A ferroelectric tetragonal phase exists on the $PbTiO_3$-rich side. In the composition of Zr:Ti≈1:1, the PZT ceramics are characterized by a morphotropic phase boundary (MPB) on which tetragonal and rhombohedral phases coexist without a solubility gap [2]. As PZT ceramics usually exhibit their maximum values of the relative dielectric permittivity and the electromechanical coupling coefficients close to the MPB [3], they have been widely used in piezoelectric transducers. Besides, a phase transition from a higher temperature rhombohedral ferroelectric phase [$F_{R(HT)}$] to a lower temperature rhombohedral ferroelectric form [$F_{R(LT)}$] was observed for mol fractions of $PbTiO_3$ in the range 0.06 to 0.37 [3–5] The latter has the oxygen octahedra tilted about to [111] direction while the former has no tilting. Since this transition between the two ferroelectric phases occurs at a low temperature and appears as a step in spontaneous polarization, P_s, rhombohedral PZT ceramics have been suggested for application in pyroelectric detectors [4].

Various transition temperatures in the PZT solid solutions have been theoretically calculated using thermodynamic formalisms based on the Landau–Devonshire phenomenological theory [6–8]. Haun and coworkers evaluated various coefficients related to the free energy function and simulated phase diagrams in the absence of pressure [7]. Recently, the pressure dependence of the phase stability has been calculated by Yamamoto et al. [8]. However, the $F_{R(LT)}$–$F_{R(HT)}$ transition in the presence of stress has not been studied up to now. This is because the rotostrictive coefficients related to the coupling between the oxygen octahedron and the stress have not been estimated.

In this study, phenomenological free energy functions were developed first, and the rotostrictive coefficient $R_h(=R_{11}+2R_{12})$ was evaluated to investigate the effects of hydrostatic pressure on the $F_{R(LT)}$–$F_{R(HT)}$ transition. On the basis of these results, the pressure dependence of phase transitions in the PZT system was predicted, and a three-dimensional phase diagram was simulated using temperature, composition and stress as the three independent thermodynamic variables.

* Corresponding author.

0272-8842/00/$20.00
PII: S0272-8842(99)00096-6

2. Phenomenological thermodynamic function

The elastic Gibbs free energy function based on the Landau–Devonshire phenomenological thermodynamic theory can be expressed using Taylor series in powers of polarization, stress and tilt angle of oxygen octahedron in the absence of antiferroelectric polarization as [7]:

$$\begin{aligned}\Delta G = {} & \alpha_1(P_1^2+P_2^2+P_3^2)+\alpha_{11}(P_1^4+P_2^4+P_3^4)\\ & +\alpha_{12}(P_1^2P_2^2+P_2^2P_3^2+P_3^2P_1^2)+\alpha_{111}(P_1^6+P_2^6+P_3^6)\\ & +\alpha_{112}\left[P_1^4(P_2^2+P_3^2)+P_2^4(P_3^2+P_1^2)+P_3^4(P_1^2+P_2^2)\right]\\ & +\alpha_{123}P_1^2P_2^2P_3^2+\beta_1(\theta_1^2+\theta_2^2+\theta_3^2)+\beta_{11}(\theta_1^4+\theta_2^4+\theta_3^4)\\ & +\gamma_{11}(P_1^2\theta_1^2+P_2^2\theta_2^2+P_3^2\theta_3^2)+\gamma_{12}\left[P_1^2(\theta_2^2+\theta_3^2)\right.\\ & \left.+P_2^2(\theta_3^2+\theta_1^2)+P_3^2(\theta_1^2+\theta_2^2)\right]+\gamma_{44}(P_1P_2\theta_1\theta_2\\ & +P_2P_3\theta_2\theta_3+P_3P_1\theta_3\theta_1)-1/2S_{11}(X_1^2+X_2^2+X_3^2)\\ & -S_{12}(X_1X_2+X_2X_3+X_3X_1)-1/2S_{44}(X_4^2+X_5^2+X_6^2)\\ & -Q_{11}(X_1P_1^2+X_2P_2^2+X_3P_3^2)-Q_{12}\left[X_1(P_2^2+P_3^2)\right.\\ & \left.+X_2(P_3^2+P_1^2)+X_3(P_1^2+P_2^2)\right]-Q_{44}(X_4P_2P_3\\ & +X_5P_3P_1+X_6P_1P_2)-R_{11}(X_1\theta_1^2+X_2\theta_2^2+X_3\theta_3^2)\\ & -R_{12}[X_1(\theta_2^2+\theta_3^2)+X_2(\theta_3^2+\theta_1^2)+X_3(\theta_1^2+\theta_2^2)]\\ & -R_{44}(X_4\theta_2\theta_3+X_5\theta_3\theta_1+X_6\theta_1\theta_2)\end{aligned} \tag{1}$$

where P_i is the magnitude of the polarization vector along the direction i, α_1 the dielectric stiffness, α_{ij}, α_{ijk} the high-order stiffness coefficients at constant stress, β_1, β_{11} the octahedral torsion coefficients, γ_{ij} the coupling coefficients between the polarization and tilt angle (θ), S_{ij} the elastic compliances measured at constant polarization, Q_{ij} the electrostrictive coefficients written in polarization notation, and R_{ij} the rotostrictive coefficients written in tilt angle notation. In the reduced notation, X_1, X_2, X_3 denote the tensile stresses and X_4, X_5, X_6 the shear components. The dielectric stiffness constant, α_1, is assumed to be a linear function of temperature near the Curie temperature (the Curie–Weiss law). All other coefficients are assumed to be independent of temperature [6–8]. Their optimized values are given in a series of papers reported by Haun and coworkers except for the rotostrictive coefficients [7,9]. Values related to the rotostrictive coefficients (R_{11}, R_{12}) will be evaluated in Section 3.

To investigate thermodynamically stable phase fields at a given hydrostatic pressure, one should consider Eq. (1) under the following conditions:

$$X_1 = X_2 = X_3 = \sigma, \qquad X_4 = X_5 = X_6 = 0.$$

Then, the free energy function becomes

$$\begin{aligned}\Delta G = {} & a_1(P_1^2+P_2^2+P_3^2)+\alpha_{11}(P_1^4+P_2^4+P_3^4)\\ & +\alpha_{12}(P_1^2P_2^2+P_2^2P_3^2+P_3^2P_1^2)+\alpha_{111}(P_1^6+P_2^6+P_3^6)\\ & +\alpha_{112}\left[P_1^4(P_2^2+P_3^2)+P_2^4(P_3^2+P_1^2)+P_3^4(P_1^2+P_2^2)\right]\\ & +\alpha_{123}P_1^2P_2^2P_3^2+\beta_1(\theta_1^2+\theta_2^2+\theta_3^2)+\beta_{11}(\theta_1^4+\theta_2^4+\theta_3^4)\\ & +\gamma_{11}(P_1^2\theta_1^2+P_2^2\theta_2^2+P_3^2\theta_3^2)+\gamma_{12}\left[P_1^2(\theta_2^2+\theta_3^2)\right.\\ & \left.+P_2^2(\theta_3^2+\theta_1^2)+P_3^2(\theta_1^2+\theta_2^2)\right]+\gamma_{44}(P_1P_2\theta_1\theta_2\\ & +P_2P_3\theta_2\theta_3+P_3P_1\theta_3\theta_1)-3/2(S_{11}+2S_{12})\sigma^2\\ & -(Q_{11}+2Q_{12})(P_1^2+P_2^2+P_3^2)\sigma-(R_{11}+2R_{12})\\ & (\theta_1^2+\theta_2^2+\theta_3^2)\sigma\end{aligned} \tag{2}$$

We can now derive various relations as to ferroelectric properties using the above equation and appropriate boundary conditions. First, each relevant phase in the PZT system must satisfy the following conditions:

- Cubic P_c
  $P_1^2 = P_2^2 = P_3^2 = 0, \qquad \theta_1^2 = \theta_2^2 = \theta_3^2 = 0$
- Tetragonal F_T
  $P_1^2 = P_2^2 = 0, \qquad P_3^2 \neq 0, \qquad \theta_1^2 = \theta_2^2 = \theta_3^2 = 0$
- High-temperature rhombohedral $F_{R(HT)}$
  $P_1^2 = P_2^2 = P_3^2 \neq 0, \qquad \theta_1^2 = \theta_2^2 = \theta_3^2 = 0$
- Low-temperature rhombohedral $F_{R(LT)}$
  $P_1^2 = P_2^2 = P_3^2 \neq 0, \qquad \theta_1^2 = \theta_2^2 = \theta_3^2 \neq 0$

The elastic Gibbs free energy (ΔG), the spontaneous polarization (P_3) and the tilt angle (θ_3) of each phase can be derived from the above conditions using the stability conditions ($\partial\Delta G/\partial P_3 = 0$, $\partial\Delta G/\partial\theta_3 = 0$), as shown below:

- Cubic P_c
  $$\Delta G = -\frac{3}{2}[s_{11}+2s_{12}]\sigma^2 \tag{3}$$
- Tetragonal F_T
  $$P_3^2 = \frac{-\alpha_{11}+\left[\alpha_{11}^2-3\alpha_{111}(\alpha_1-Q_h\sigma)\right]^{\frac{1}{2}}}{3\alpha_{111}} \tag{4}$$
  $$\Delta G = -\frac{3}{2}(s_{11}+2s_{12})\sigma^2+(\alpha_1-Q_h\sigma)P_3^2 + \alpha_{11}P_3^4+\alpha_{111}P_3^6 \tag{5}$$

- High-temperature rhombohederal $F_{R(HT)}$

$$P_3^2 = \frac{-\zeta + \left[\zeta^2 - 9\xi(\alpha_1 - Q_h\sigma)\right]^{\frac{1}{2}}}{3\xi} \tag{6}$$

$$\Delta G = -\frac{3}{2}(s_{11} + 2s_{12})\sigma^2 + 3(\alpha_1 - Q_h\sigma)P_3^2 + \zeta P_3^4 + \xi P_3^6 \tag{7}$$

- Low-temperature rhombohederal $F_{R(LT)}$

$$P_3^2 = \frac{-\zeta + \left[\zeta^2 - 9\xi(\alpha_1 - Q_h\sigma + \phi\theta_3^2)\right]^{\frac{1}{2}}}{3\xi} \tag{8}$$

$$\theta_3^2 = \frac{-\beta_1 - \phi P_3^2 + R_h\sigma}{2\beta_{11}} \tag{9}$$

$$\Delta G = -\frac{3}{2}(s_{11} + 2s_{12})\sigma^2 + 3(\alpha_1 - Q_h\sigma)P_3^2 + \zeta P_3^4 + \xi P_3^6 + 3(\beta_1 - R_h\sigma)\theta_3^2 + 3\beta_{11}\theta_3^4 + 3\phi P_3^2\theta_3^2 \tag{10}$$

where $Q_h = Q_{11} + 2Q_{12}$, $R_h = R_{11} + 2R_{12}$, $\varphi = \gamma_{11} + 2\gamma_{12} + \gamma_{44}$, $\zeta = 3(\alpha_{11} + \alpha_{12})$, $\xi = 3\alpha_{111} + 6\alpha_{112} + \alpha_{123}$.

The above equations relate P_3, θ_3 and ΔG to the coefficients of the energy function. Thus, the free energy of each phase can be calculated if these coefficients are determined. Most of the relevant coefficients have been reported previously [7,9], but the rotostrictive coefficient (R_h) has not been determined yet. Therefore, we will evaluate R_h in the next section and calculate the pressure dependence of the thermodynamically stable phase fields in Section 4.

3. Evaluation of the rotostrictive coefficient R_h

The rotostrictive constant $R_h(= R_{11} + 2R_{12})$ is a coefficient for the tilt angle and stress. These two variables are coupled so as to make a contribution to the free energy. Therefore, it can be said that the spontaneous strain x_i is contributed by the tilt angle. Using the relation of $x_i = -\partial\Delta G/\partial X_i$, the elastic spontaneous strains of rhombohedral phases can be derived from Eq. (1) under zero stress conditions as follows:

- High-temperature rhombohedral $F_{R(HT)}$

$$x_1 = x_2 = x_3 = (Q_{11} + 2Q_{12})P_3^2 = Q_hP_3^2 \tag{11}$$

- Low-temperature rhombohedral $F_{R(LT)}$

$$x_1 = x_2 = x_3 = (Q_{11} + 2Q_{12})P_3^2 + (R_{11} + 2R_{12})\theta_3^2 = Q_hP_3^2 + R_h\theta_3^2 \tag{12}$$

Since Q_h has already been reported, R_h can be evaluated from Eqs. (8), (9) and (12) if the spontaneous normal strain x_i ($i = 1, 2, 3$) is taken in the absence of pressure. The normal strain is generally calculated using the following relation:

$$x_i = (a - a_0)/a_0 \tag{13}$$

where a is the lattice constant of the rhombohedral structure, and a_0 is the lattice constant of the assumed cubic structure that should not have been transformed into the rhombohedral one. Therefore, if a_0 is determined, R_h can be evaluated.

We have done the above described procedure using the experimental data of $Pb(Zr_{0.9}Ti_{0.1})O_3$ single crystal, as measured by Glazer et al. [4]. Fig. 1 shows the lattice constant of the assumed cubic structure in the high-temperature rhombohedral region. They were obtained by applying the experimental lattice constants to Eq. (11). The solid curve is the fit extrapolated into the low-temperature rhombohedral region using these data. We have computed a_0 of the low-temperature rhombohedral structure from this fit and have estimated the temperature dependence of R_h (Table 1). From 40 to 60°C R_h is slightly dependent on temperature, but the magnitude of R_h increases significantly as temperature

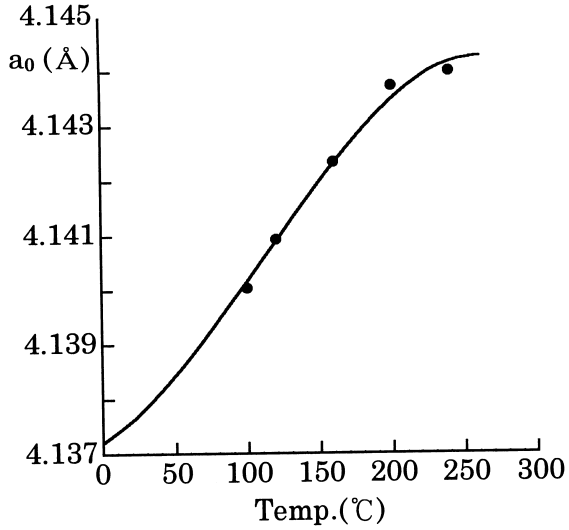

Fig. 1. Lattice constant of the assumed cubic structure versus temperature in the rhombohedral $Pb(Zr_{0.9}Ti_{0.1})O_3$. The data points were calculated from the experimental lattice constants and the solid curve is the fit using these data.

approaches the transition point to the high-temperature rhombohedral phase. However, we have simply assumed that R_h is 1.553×10^{-4} deg.$^{-2}$ and that it is independent of temperature and composition, as was done by other investigators [7].

The experimental data of the lattice constant [4] and the fit using R_h given above are plotted in Fig. 2. It should be noted that there is a break in the curve. This indicates that the first-order transition characteristics are theoretically realized and that the fit agrees with the experimental data.

4. Hydrostatic pressure dependence of phase transitions

The phase diagram of PZT under a given hydrostatic pressure was simulated using the following conditions: $\Delta G_{FT} = \Delta G_{FR(HT)}$ at the MPB, $\Delta G_{Pc} = \Delta G_{FR(HT)}$ or $\Delta G_{Pc} = \Delta G_{FT}$ at the Curie temperature, and $\Delta G_{FR(LT)} = \Delta G_{FR(HT)}$ at the $F_{R(LT)}-F_{R(HT)}$ transition. In the estimate of ΔG, we have used the reported values for $\alpha_{ijk}, \beta_{ij}, Q_{ij}, S_{ij}, \varphi$ [7]. On the other hand, we have used the value evaluated in this study for R_h. Fig. 3 presents a three-dimensional phase diagram of the PZT solid solution system under tensile hydrostatic pressure using composition, pressure and temperature as the three independent variables. Similarly, Fig. 4 shows a two-dimensional representation of the computed three-dimensional phase diagram. With increasing tensile pressure, the Curie temperature increases but the $F_{R(LT)}-F_{R(HT)}$ transition temperature decreases, and the MPB composition moves slightly towards the tetragonal phase field. It can be said that the stability of the high temperature rhombohedral phase field is enhanced by tensile hydrostatic pressure (Fig. 4) because its structure has the largest lattice parameter. The figure also shows that the Curie temperature near the composition of Zr:Ti≈1:1 is deviated from the general tendency.

Table 1
Values of the rotostrictive coefficient R_h at three different temperatures in the low temperature rhombohedral region

Temperature (°C)	40	60	80
R_h (deg.$^{-2}$)	-1.4880×10^{-4}	-1.5032×10^{-4}	-1.6169×10^{-4}

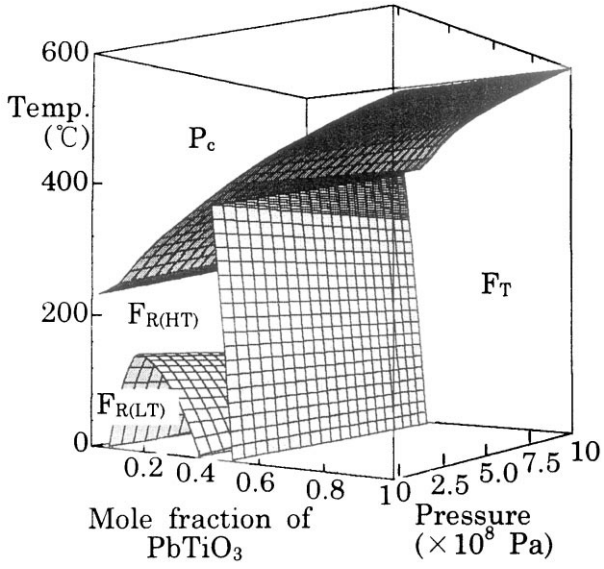

Fig. 3. Three-dimensional representation of the thermodynamically stable fields of PZT under tensile hydrostatic pressure.

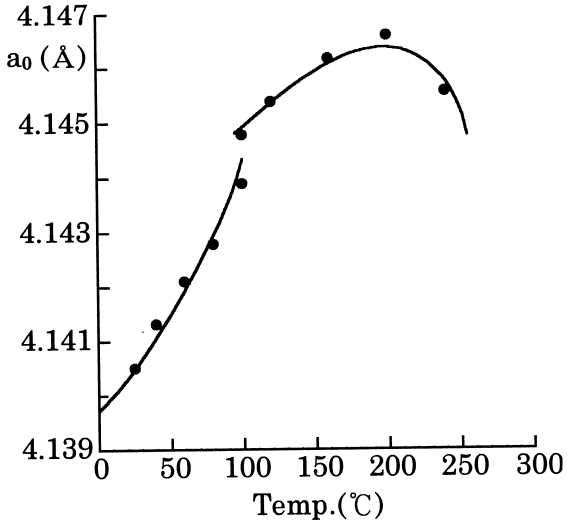

Fig. 2. Lattice constant of the rhombohedral $Pb(Zr_{0.9}Ti_{0.1})O_3$ versus temperature. The points are the experimental data and the solid curves are the theoretical fits of the data.

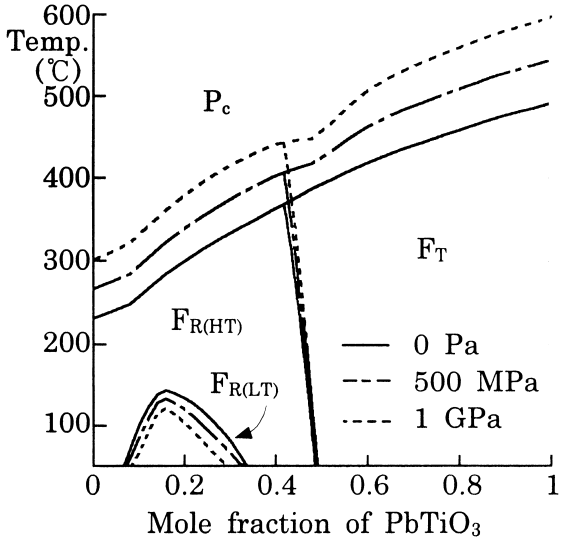

Fig. 4. The computed phase diagram of the PZT system, showing the effects of tensile hydrostatic pressure on various phase transitions.

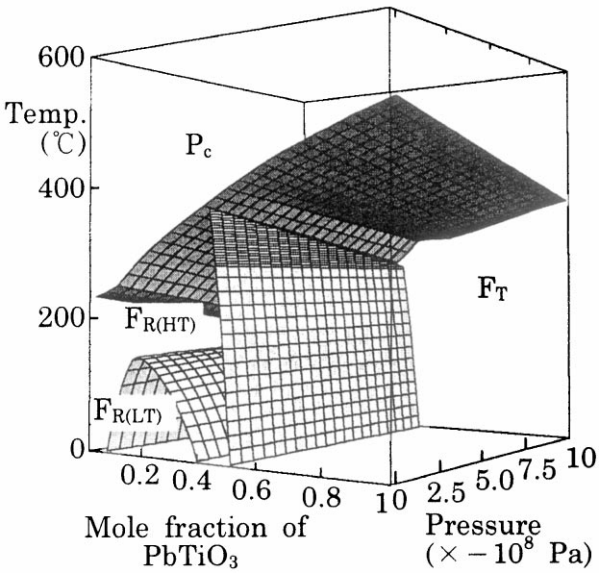

Fig. 5. Three-dimensional representation of the thermodynamically stable fields of PZT under compressive hydrostatic pressure.

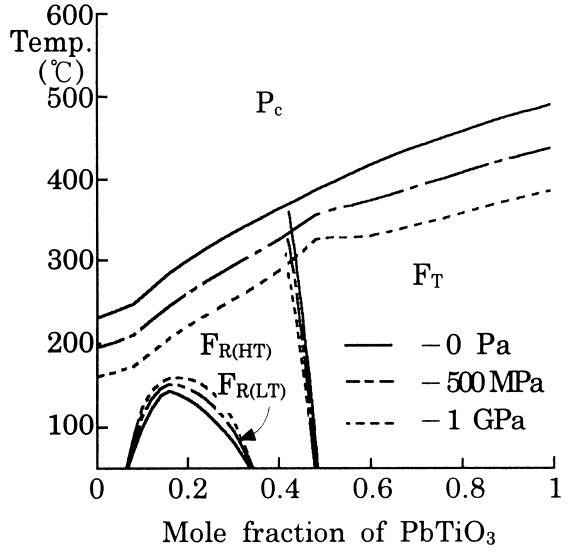

Fig. 6. The computed phase diagram of the PZT system showing the effects of compressive hydrostatic pressure on various phase transitions.

The possible cause of this could be that various phenomenological coefficients near the MPB composition were slightly mistaken and/or that higher order coefficients were neglected. Otherwise, it can be attributed to an inherent physical property of the PZT near the MPB composition. Contrary to these, opposite tendencies are predicted under compressive hydrostatic pressure. The three-dimensional phase diagram of the PZT and the two-dimensional section of the diagram under compressive hydrostatic pressure are shown in Figs. 5 and 6, respectively.

5. Conclusions

The rotostrictive coefficients (R_h) were evaluated to investigate the pressure dependence of various phase transitions in the PZT solid solution system. Using phenomenological thermodynamic formalism we have predicted a shift of the thermodynamically stable phase fields of PZT under hydrostatic pressure. We have further simulated a three-dimensional phase diagram using composition, pressure and temperature as the three independent thermodynamic variables. It is predicted that the high temperature rhombohedral phase becomes more stable than the low temperature phase under tensile hydrostatic pressure. Contrary to this, an opposite trend becomes evident with increasing compressive pressure.

References

[1] L.E. Cross, Ceram. Bull. 63 (1984) 586.
[2] W. Cao, L.E. Cross, Phys. Rev. B 47 (1993) 4825.
[3] B. Jaffe, W.R. Cook Jr., H. Jaffe, Piezoelectric Ceramics, Academic, New York.
[4] R. Clarke, A.M. Glazer, Ferroelectrics 12 (1976) 207.
[5] T.R. Halemane, M.J. Haun, L.E. Cross, R.E. Newnham, Ferroelectrics 62 (1985) 149.
[6] A. Amin, R.E. Newnham, L.E. Cross, Phys. Rev. B 34 (1986) 1595.
[7] M.J. Haun, E. Furman, S.J. Jang, L.E. Cross, Ferroelectrics 99 (1989) 13.
[8] T. Yamamoto, Y. Makino, Jpn J. Appl. Phys. 35 (1996) 3214.
[9] M.J. Haun, Z.Q. Zhuang, E. Furman, S.J. Jang, L.E. Cross, J. Am. Ceram. Soc. 72 (1989) 1140.